NJC

Accepted Manuscript

This is an *Accepted Manuscript*, which has been through the Royal Society of Chemistry peer review process and has been accepted for publication.

Accepted Manuscripts are published online shortly after acceptance, before technical editing, formatting and proof reading. Using this free service, authors can make their results available to the community, in citable form, before we publish the edited article. We will replace this *Accepted Manuscript* with the edited and formatted *Advance Article* as soon as it is available.

You can find more information about *Accepted Manuscripts* in the Information for Authors.

Please note that technical editing may introduce minor changes to the text and/or graphics, which may alter content. The journal's standard Terms & Conditions and the Ethical guidelines still apply. In no event shall the Royal Society of Chemistry be held responsible for any errors or omissions in this *Accepted Manuscript* or any consequences arising from the use of any information it contains.

ROYAL SOCIETY OF CHEMISTRY

www.rsc.org/njc

Green synthesis of graphene-silver composites reduced by L-ascorbic acid/water vapor for SERS enhancement and antibacterial application

Jian Liu[a], Libin Liu[a*] Xiwen Wu[a], Xiaokai Zhang[b], Tianduo Li[a*]

[a] Shandong Provincial Key Laboratory of Fine Chemicals, Key Laboratory of Fine Chemicals in Universities of Shandong, Qilu University of Technology，Jinan 250353, China

[b] Institute of Semiconductors, Shandong Normal University, No. 88 East Culture Road, Jinan, China

Abstract

A green approach for the preparation of reduced graphene oxide (RGO) film was developed by using L-ascorbic acid/water vapor as reducing agent. Except hydrazine hydrate vapor or hydroiodic acid vapor, it is the first time to use environment-friendly reducing agent vapor to reduce graphene oxide (GO) films into RGO films. The as-prepared RGO films are flexible and exhibit high electrical conductivity up to 3500 S m^{-1}. Moreover, the L-ascorbic acid/water vapor can penetrate into the GO films and reduce the silver ions. The as-reduced RGO/Ag composite film can be utilized as an effective surface-enhanced Raman scattering active substrate and the signals of Raman can be adjusted by changing the mass of the silver ions. Furthermore, the RGO/Ag composites also showed different antibacterial activity against *E. coli*, *S. aureus* and *white-rot fungi*. This work provides a straight-forward and green approach to fabricating RGO/Ag composites useful in bio-application as well as material science.

* *Corresponding authors*: Fax: +86 531 89631208.

E-mail addresses: lbliu@qlu.edu.cn (L. B. Liu), litianduo@163.com (T. D. Li).

1. Introduction

Recently, research on ultrathin 2-D graphene sheet has attracted great attention because of its unique electronic, mechanical, optical and thermal properties [1-3]. These excellent physical and chemical properties make it promising for potential applications in many technological fields, such as nanoelectronics [4], composites [5] and energy storage devices [6]. There are several methods for preparing graphene, including micromechanical cleavage [7], chemical vapor deposition [8-10], liquid-phase exfoliation of graphite [11] and chemical reduction of graphene oxide (GO) [12, 13]. Among these, the chemical reduction of GO is considered as a versatile method that is suited to large-scale production and functionalization. In most of the cases, strong reducing agents, such as hydrazine monohydrate, hydroquinone, sodium borohydride ($NaBH_4$), hydroxylamine, phenylenediamine, and hydroiodic acid, have been used as reducing agents [14-19]. However, these reducing chemicals are highly toxic, strong corrosive and explosive, and may damage the environment or be cost-prohibitive when they are used for the large scale production of graphene. Moreover, the presence of trace amounts of such toxic agents could have detrimental effect, especially on bio-related application. To overcome the above problems, some green nanotechnologies were also reported about reduction of GO by using sugar, caffeic acid, and protein bovine serum albumin as reducing agents [20-23]. Generally, with eco-friendly reducing agents, the reduction of GO is successfully demonstrated to alleviate the environmental issues. However, these reduction processes were almost conducted in solution states, pure RGO films were difficult to obtain due to the absorption of reducing agent on graphene sheets, which may affect the properties in later applications. Up to now, few reports are related to the reduction of GO film on the solid substrate.

Since graphene films are commonly supported on substrates, direct reduction of GO films on substrates without considering the solubility is extremely important for practical applications. However, both hydrazine and $NaBH_4$ are not suitable for the reduction of GO films, especially for those needing high flexibility for applications in

flexible devices, due to the stiffening and disintegration of the films during reduction [24]. It has also been reported that hydroiodic acid can efficiently reduce GO on solid substrates to highly conductive graphene without damaging the GO films [14, 25]. However, utilization of toxic and corrosive reagents limits their applications. Therefore, there is a need to develop a simple, low cost, and green route to prepare RGO films without destroying their original high flexibility and integrity.

Here, we demonstrate that L-ascorbic acid (L-AA)/water vapor is used as reducing agent to reduce GO films. L-AA is a natural antioxidant essential for many metabolic functions in living organisms and widely employed as a food additive as reducing agent [26-28]. In our case, we use L-AA/water vapor as a reducing agent to directly reduce GO films into graphene films. More importantly, the L-ascorbic acid/water vapor also can reduce the silver ion into silver nanoparticles. The as-prepared RGO/silver composites not only can be used as surface enhanced Raman scattering active substrates but also own the antibacterial ability.

2. Experimental sections

2.1 Materials

Graphite powder (8000 mesh, purity 99.95%), sodium nitrate ($NaNO_3$), silver nitrate ($AgNO_3$), Rhodamine B (RhB) and L-ascorbic acid were purchased from Aladdin Chemistry Co. Ltd. Sulfuric acid (H_2SO_4), potassium permanganate ($KMnO_4$), hydrogen peroxide (H_2O_2) were obtained from Sinopharm Chemical Reagent Co. Ltd.

2.2 Preparation of GO Suspension Solution

Graphene oxide was prepared from natural graphite powder according to modified Hummers method. Briefly, graphite powder (1 g) and $NaNO_3$ (0.75 g) were put into a three-necked 250 ml flask with H_2SO_4 (34 mL). A strong agitation at 0 °C in an ice water bath for 20 min was needed. $KMnO_4$ (5 g) was slowly added for 10 min. After heating the flask for 2 h at 40 °C, the highly sticky liquid was obtained. Then, the system was cooled down to 35 °C and was stirred for 30 min. After the reaction went to completion, D.I. water (50 ml) and H_2O_2 (5 mL, 5 % w/v) were added to the resulting solution when the mixture was cooled down to room temperature. The

graphite oxide was centrifuged and washed with water until the pH of the filtrate was neutral. Finally, graphite oxide precipitate was redispersed in water by sonication at frequency of 40 kHz and power of 150 W for 1 h, then GO suspension was obtained.

2.3 Fabrication of Reduced Graphene Oxide Paper

The GO paper was fabricated through vacuum filtration of the GO aqueous dispersion (2 mg) by using a cellulose ester membrane (50 mm in diameter, 0.22 μm pore size). For reduction, the GO paper on top of a glass bottle was placed in a Teflon lined autoclave in which different concentration of L-AA aqueous solution was added. The GO film did not directly contact with the aqueous solution. Finally, the autoclave was heated at 100 °C for 48 h to obtain RGO paper.

2.4 Fabrication of RGO/Ag Composite Films

Different mass of silver nitrate was added in the GO aqueous dispersion to make a homogeneous solution by sonication. The Ag^+ would be absorbed on GO sheet by ionic interaction. The Ag^+-GO films was obtained by vacuum filtration of Ag^+-GO aqueous dispersion. The RGO/Ag composite films were fabricated by L-AA/water vapor treatment which is the same as the reduction of GO films. The composite films with different mass ratios of Ag^+/GO (2:1, 5:1 and 10:1) are marked as Ag2G1, Ag5G1 and Ag10G1, respectively. These composite films after L-AA/water vapor treatment were immersed into D.I. water for 5 min for washing and separation. Then the free-standing RGO/Ag composite films were obtained by peeling off from the cellulose ester membrane. These films are stable in water and dried for SERS and antimicrobial experiments.

2.5 SERS Measurements

6 μl of 10^{-3} M RhB in ethanol was dropped on Ag2G1, Ag5G1 and Ag10G1, respectively, and then was left to dry at room temperature for SERS measurements. To further characterize the detection limit of Ag10G1, 10^{-6} M RhB ethanol solution was used. The Raman spectra were performed by using a LabRAM HR800 Raman spectrometer (HORIBA JY, France). An excitation laser wavelength of 633 nm, a power of 5 mW and a focused laser beam spot of around 1 μm in diameter were used. The acquisition time for each Raman spectra was 20 s. The Raman spectra were

obtained by measuring five different positions of each sample.

2.6 Antimicrobial Assays

Antimicrobial activity of RGO/Ag composites were tested against the microbial strains: Gram-negative *Escherichia coli* (*E. coli*), Gram-positive *Staphylococcus aureus* (*S. aureus*), and *White-rot fungi*. For comparative studies, the antimicrobial activity of RGO was also taken into account. For antibacterial tests, all petri dishes and materials were sterilized in a pressure cooker before experiments. The bacteria were stored in 15% (v/v) glycerin solution at -80 °C and were grown in Luria–Bertani (LB) and potato dextrose (PD) medium with agitation at 37 °C overnight. The bacteria were spread onto LB-agar or PD-agar plates incubated at 37 °C for 24 h. Then the zone of inhibition was observed.

3. Results and discussion

3.1 Reduction of graphene oxide by L-ascorbic acid/water vapor

The GO paper was first fabricated through vacuum filtration of the GO aqueous dispersion and then put in a sealed autoclave (Fig. 1A). After L-ascorbic acid/water vapor treatment for 48 h, a first indication of the reduction is the color change of GO film from brownish yellow to black, suggesting the restoration of aromatic graphene structure [29]. The contact angle greatly increases from ~37.2^{o} for GO paper to ~88.8^{o} for RGO paper, which is in agreement with the previous work [30], due to their becoming less hydrophilic as a result of oxygen removal (see discussed below) (Figure S1). The thickness of the filtered film can be adjusted from dozen of nanometers to tens of micrometers by the volume and concentration of dispersion. If the thickness reaches to one micrometer, they can be peeled off the membrane to form free-standing or paper-like films as shown in Figure 1B.

To quantitatively investigate the effect of reduction, the GO film was reduced from vapors of the different concentration of the L-ascorbic acid solution. The UV−vis spectrum of GO solution exhibits two characteristic features: a maximum at 233 nm, which can be attributed to $\pi \rightarrow \pi^*$ transition of aromatic C−C bond; and a shoulder at 300 nm corresponding to $n \rightarrow \pi^*$ transition of C=O bonds (Fig. 1C). After

L-AA/water vapor treatment, the absorption peak was red-shifted to 254 nm and the shoulder of the C=O bond disappeared by using the vapor of low concentration of L-AA solution. With an increase in the concentration of L-AA solution up to 4 mg/ml, the peak was shifted slightly to 269 nm and a significant increase in absorbance tail in the visible region (>300 nm) was noticed. These effects indicate that the electronic conjugation within the carbon framework of the graphene nanosheets has been restored upon L-AA/water vapor reduction, which is in agreement with the previous reports [31, 32]. Little increase in the absorption was found when the concentration was further increased. Hence, the concentration was fixed to 4 mg/ml for later experiment.

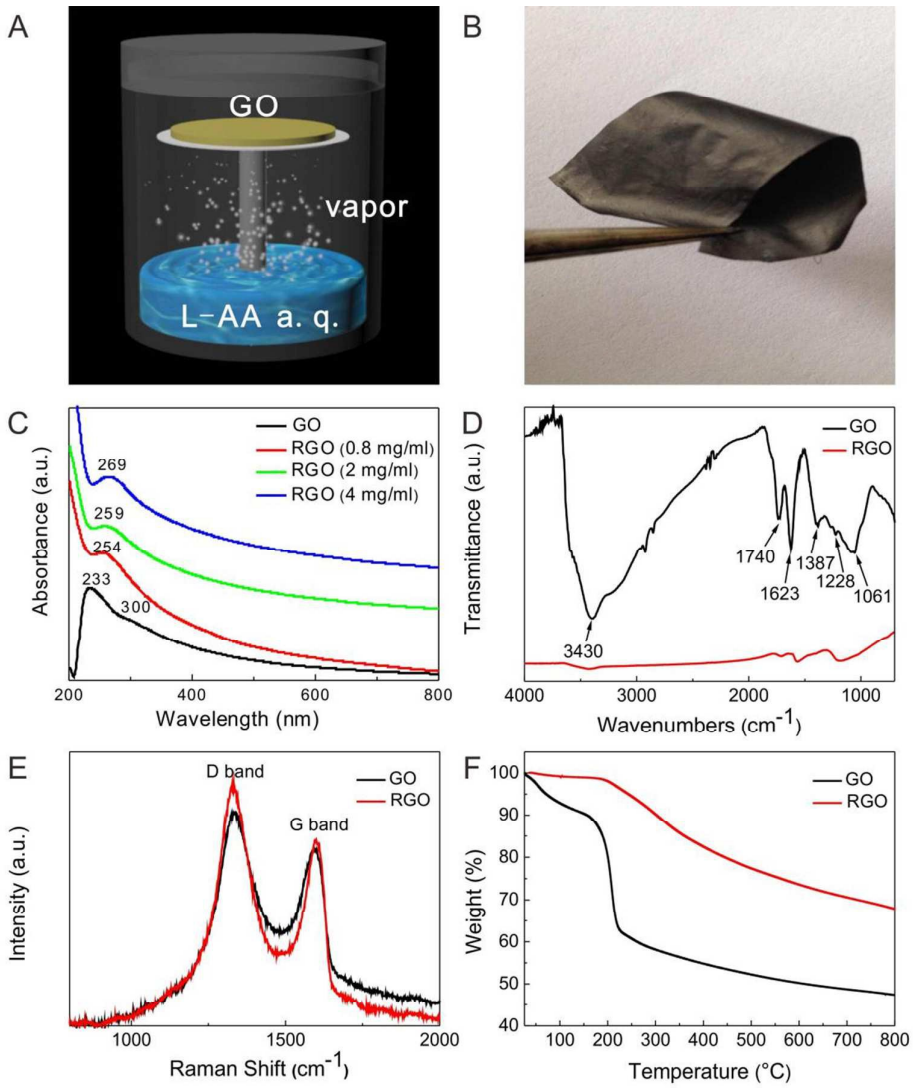

Figure 1. (A) Schematic of the reaction system; (B) a free-standing and flexible RGO

film; (C) UV-vis absorption spectra of GO aqueous dispersions and RGO films reduced via different concentration of L-AA in water at 100 °C for 48 hours; (D) FT-IR spectra of GO and RGO samples; (E) Raman spectra of GO and RGO samples; (F) TGA plots of GO and RGO.

The reduction of the oxygen-containing groups in GO by L-AA/water vapor was also confirmed by FT-IR spectroscopy (Fig. 1D). For GO sheet, the broad peak in the frequency range of 3200–3500 cm^{-1} is ascribed to the O–H stretching vibration and the peak at 1740 cm^{-1} is attributed to the C=O stretching vibration. The sharp peak at 1623 cm^{-1} corresponds to the C=C stretching vibration. The absorption peaks located at 1228 and 1061 cm^{-1} are ascribed to the epoxy C–O and alkoxy C–O stretching vibrations, respectively. The peak at 1387 cm^{-1} arises from the bending vibration of O–H groups [33, 34]. After L-AA/water vapor reduction, the intensities of all FTIR peaks correlated to the oxygenous groups decrease dramatically and the oxygenated species of O-C=O and C=O are substantially removed, indicating that GO nanosheets have been reduced to RGO nanosheets.

Raman spectrum is one of the most widely used techniques to characterize the electronic and structural properties of graphitic materials. In our case, the Raman spectra of GO and RGO reveal two prominent peaks at G band and D band. The G band at 1570–1600 cm^{-1} is corresponding to the first-order scattering of E_{2g} mode, and the D band at about 1330 cm^{-1} arises from a breathing mode of Κ-point phonons of A_{1g} symmetry. The D band is related to the amount of disorder and its intensity shows the degree of edge chirality. The intensity ratio of G and D bands of RGO indicates the degree of the disorder such as defects, ripples and edges [19]. As shown in Figure 1E, the I_D/I_G intensity ratio of GO was calculated to be 1.12. After reduction, the intensity was increased to 1.51. This number is similar to those calculated from the reduction by hydrazine in previous works ($I_D/I_G \sim 1.44–1.63$ [35, 36]), which suggests restoration of the graphitic sp^2 network by removing oxygen-containing functional groups.

The successful reduction of GO film was also reflected in the TGA curves (Fig.

1F). GO is thermally unstable at elevated temperature and starts to lose mass (about 7.2% weight) upon heating to 100 ^{o}C. This is due to the loss of residual water between the adjacent hydrophilic GO sheets. A sharper mass loss occurs at ~200 ^{o}C, presumably because of pyrolysis of the labile oxygen-containing functional groups [19]. After L-AA/water vapor reduction, RGO exhibits a prominent thermal stability in inert nitrogen atmosphere and with removal of the thermally labile oxygen functional groups starts from 200 ^{o}C. However, there is still significant mass loss for RGO between 300-800 ^{o}C, in agreement with the previous report [37], suggesting that even the reduction process cannot remove the most stable functionalities.

It should be noted that the RGO paper was obtained by immersing into D.I. water for washing and peeling off from the cellulose ester membrane. This process ensures removal of any absorbed L-AA completely because of highly dissolvable L-AA into water. Furthermore, the UV-vis, FTIR and XPS data indicate the reduction of GO into RGO and do not show any singles of L-AA. Therefore, the mass loss in the TGA results should be due to the left oxygen containing functional groups on RGO sheets after reduction.

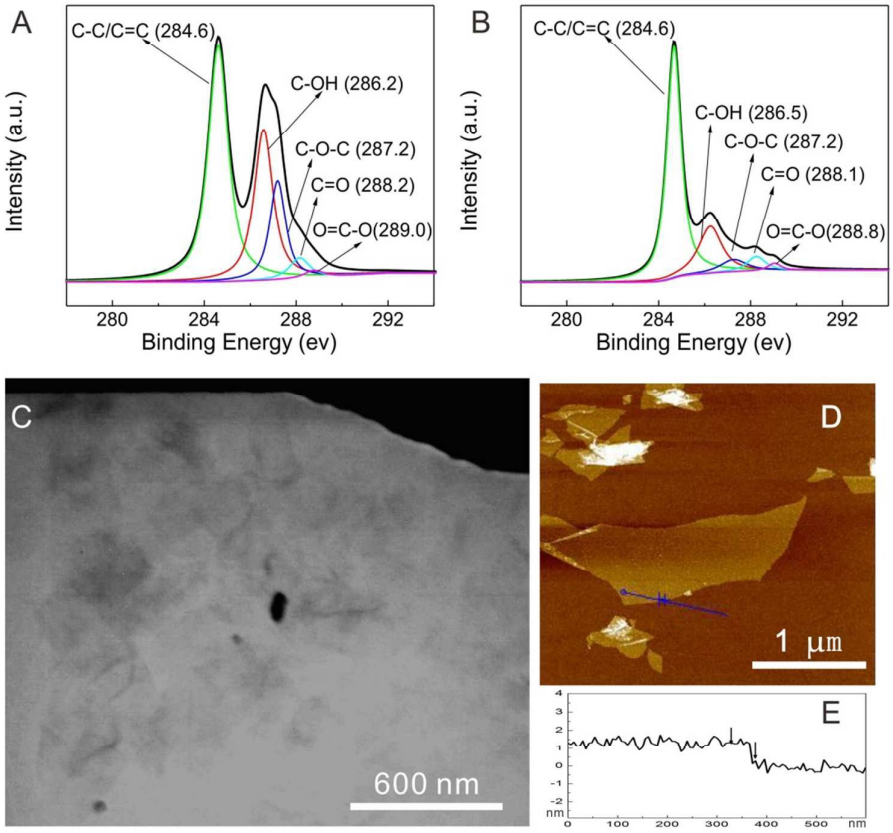

Figure 2. XPS spectra of C 1s of (A) GO and (B) RGO; (C) TEM image of RGO; (D) AFM image of RGO and (E) the height profile of the AFM image.

To further illustrate the formation of graphene, the X-ray photoelectron spectroscopy technique spectra (Fig. 2A, B and Fig. S2) were used to investigate the chemical composition and valence states of these films. The ratio of C/O is 2.1 for GO and increases to 3.2 for RGO. The reduction of oxygenous groups was further revealed in C 1s spectra. As for GO films, five different peaks centered at 284.6, 286.2, 287.2, 288.2 and 289.0 eV are observed, corresponding to C−C in unoxidized graphite carbon skeleton, C−OH in hydroxyl group, C−O−C in epoxide group, and C=O (O-C=O) in carboxyl group, respectively [38]. These peaks reveal that, compared to GO, the intensity of the C–O peak of the RGO films is significantly decreased after L-AA/water vapor reduction, revealing that a large number of oxygen-containing groups were removed and the sp^2 carbon networks were restored.

The TEM image (Fig. 2C) demonstrates that one or two transparent layers of RGO with some winkles were fabricated. A single layer of graphene sheets can be spin-coated onto silicon wafer from the dilute graphene dispersion. Tapping-mode AFM image (Fig. 2D) indicates that the thickness of graphene sheet is about 1.0 nm, which is in good agreement with the previous study [39].

The reduction mechanism of L-AA/water vapor is not clear. However, the electron withdrawing of the L-AA rings makes the hydroxyl bonds more acidic, so that the hydroxyl bonds are ready to dissociate two protons and function as nucleophiles [40, 41]. The GO sheets contain mainly two types of reactive species, including epoxide and hydroxyl. Both the epoxide and hydroxyl bonds can be opened by the oxygen anions of the L-AA through a nucleophilic attack (Fig. S3). The reduction should be also followed by a dehydration process and completed by absorbing one electron from environment. Then, the L-AA is oxidized into dehydroascorbic acid [41].

3.2 Fabrication of RGO/silver composites

It is confirmed that the oxygen-containing groups of the graphene oxide could adsorb Ag^+ or Au^+ by electrostatic interaction and then these ions could be reduced in solution by the addition of reducing agents [42, 43]. However, there are few reports related to reduce silver ion by reducing agents in the vapor states. In our case, different mass ratio of silver nitrate and GO were mixed and sonicated in aqueous dispersion, and then it was vacuum filtered on the filter paper for vapor treatment. X-ray diffraction determines the changes of interlayer distance in nanosheets shown in Figure 3A. The diffraction peak in the XRD pattern of GO appears to be 11.3^o, corresponding to the layer-to-layer distance of ~0.78 nm. It is significantly larger than that of pristine graphite (~0.34 nm). The interlayer spacing depends upon the number of oxygen-containing groups on the basal plane and the amount of water molecules absorbed in the gallery space between adjacent GO sheets [44], as indicated in the TGA curves (Fig.1F). In case of RGO, the XRD pattern exhibits a typical broad peak

centered at 23.7° (d-spacing 0.38 nm) with an obvious disappearance of the GO peaks. The broad nature of the reflection indicates the poor ordering of the sheets along the stacking direction, implying that the sample is composed mostly of single or few layers of RGO [21, 45, 46].

For RGO/Ag composites, it is observed that the d-spacing value of the synthesized Ag nanoparticles using different mass ratio of the $AgNO_3$ remains almost constant for each crystallographic plane. XRD patterns (Fig. 3B) show that the peaks for (1 1 1) and (2 0 0) planes of the Ag nanoparticles are prominent for all the $AgNO_3$ concentration range used, whereas the peaks for other three planes (2 2 0), (3 1 1), and (2 2 2) of the Ag nanoparticles could not be detected in low mass ratio (Ag2G1 and Ag5G1). The XRD patterns for Ag10G1 reveal that the prominent peak at 2 theta values of about 38.1°, 44.3°, 64.4°, 77.4° and 81.3° are assigned to the (1 1 1), (2 0 0), (2 2 0), (3 1 1) and (2 2 2) Bragg lattices of a face-centered cubic (fcc) silver crystal structure, respectively (JCPDS card no. 04-0783). The corresponding d-spacing values of the Ag nanoparticles are 2.36, 2.04, 1.46, 1.23 and 1.18 Å, respectively.

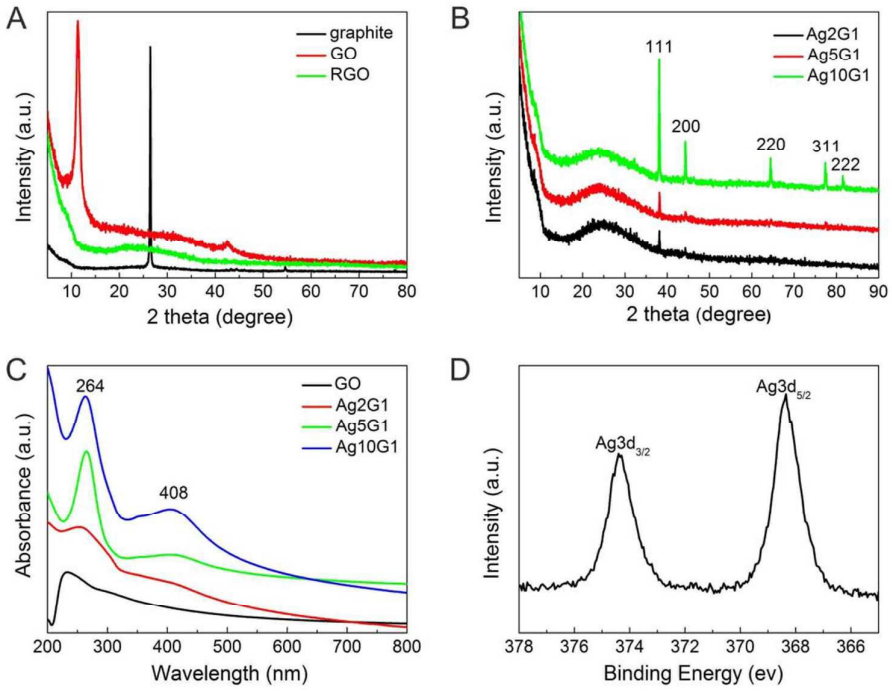

Figure 3. (A) XRD patterns of graphite, GO and RGO films; (B) XRD patterns of Ag2G1, Ag5G1 and Ag10G1 composites; (C) UV-vis absorption spectra of GO and RGO/Ag composites; (D) Typical Ag3d XPS spectra of Ag2G1 composites.

To determine the efficiency of reduction of GO with the increase of Ag^+ concentration, UV-vis spectra were carried out. The Ag2G1, Ag5G1 and Ag10G1 composite films were reduced from 8 mg/ml L-AA solution at 100 ^oC for 48 h and the UV-vis spectra of the composites were shown in Figure 3C. After L-AA/water vapor treatment, it is clearly seen that the absorption peak of GO gradually red-shifts from 233 to 264 nm, indicating the successful reduction of GO to RGO. In addition, there is a blue shift of 5 nm for the composite films compared to pure RGO films, which is the result of charge transfer interactions between RGO and silver nanoparticles. As the concentration of silver increased, a peak centered at 408 nm was observed, indicating successful reduction of silver ion into silver nanoparticles. This adsorption peak is characteristic of the surface plasmon resonance of Ag nanoparticles [47].

The typical XPS spectra of Ag2G1 composite film reveals that the ratio of C/O is about 3.1, similar to the C/O ratio of RGO (3.2). In addition, the atomic ratio of Ag in Ag2G1 was 1.2%, which indicates that a high degree of silver nanoparticles can be introduced efficiently onto the RGO sheet (Figure S2). It was reported that metallic Ag3d peaks are centered at 373.9 and 367.9 eV and Ag(I) exhibits two peaks at 375.8 and 369.6 eV [48]. For Ag2G1, the Ag3d peaks appeared at 374.3 and 368.3 eV, suggesting that there are both metallic Ag and Ag(I) adsorbed on the RGO substrate (Figure 3D). This observation may be due to that silver nanoparticles have been oxidized in the air. Note that the content of Ag(I) species compared to Ag(0) in the composites is pretty low. This is why both $Ag3d_{5/2}$ and $Ag3d_{3/2}$ in XPS spectrum showed a dominant singlet and we have failed to observe the Ag(I) peak in UV-vis absorption.

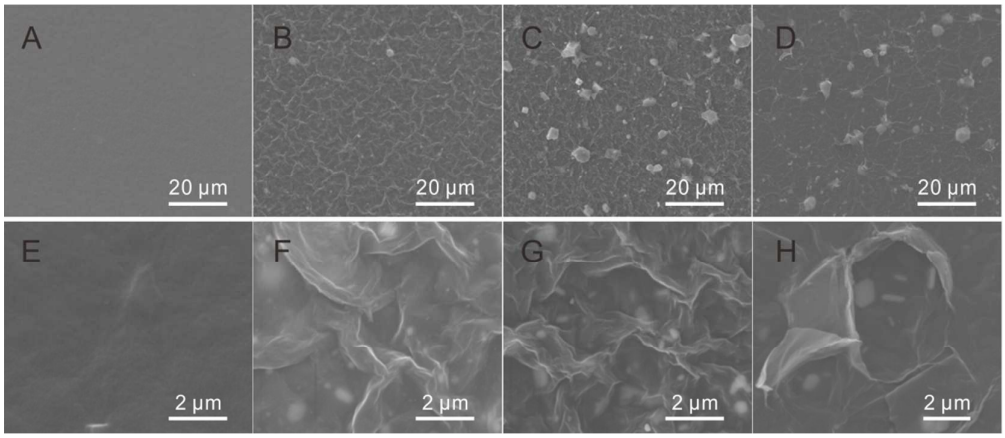

Figure 4. Typical SEM images of low and high magnification of the surface of RGO (A, E), Ag2G1 (B, F), Ag5G1 (C, G), Ag10G1 (D, H).

To investigate the morphologies changes, the surface and cross-section of the composite films were characterized by SEM. The surface of the RGO films reveal that the stacked sheets are flat, and no crumpled or curled sheets are observed (Fig. 4A, E). After the reduction of silver ions, Ag nanoparticles were completely distributed on RGO sheets, indicating a strong interaction between RGO support and Ag nannoparticles (Fig. 4). The increased water contact angles of RGO/Ag composite films, compared to RGO films, indicate that the silver nanoparticles are grown on the films surface (Fig. S1). For Ag2G1 films, the graphene sheets with silver nanoparticles look like crumpled silk waves, demonstrating that the sheets are curled. As the silver content increases, the surfaces of composites become much rougher as revealed by high magnification of SEM images, which might be attributed to the growth of nanoparticles on RGO sheets during L-AA/water vapor reduction (Fig. 4). Ag10G1 films also displayed better reflectivity compared to Ag5G1 and Ag2G1 film due to higher content of silver nanoparticles (Fig. S1). The cross-sectional SEM images reveal that the fracture edges of the RGO film exhibit a layered structure throughout the entire cross section (Fig. 5A). Compared to graphene film obtained from electrophoretic deposition and reduction [49], the film obtained from vacuum filtration of aqueous GO dispersion is more oriented and compact. After reduction of silver ions, we concluded that the layer-to-layer distance was so broadened by the

attached Ag nanoparticles between these RGO sheets. The films of the composites become more loosely as the mass of the silver ion increases (Fig. 5B-D). This also indicates that silver nanoparticles are uniformly distributed on the RGO sheet and L-AA/water vapor can penetrate into the inner of the films to carry on the reduction.

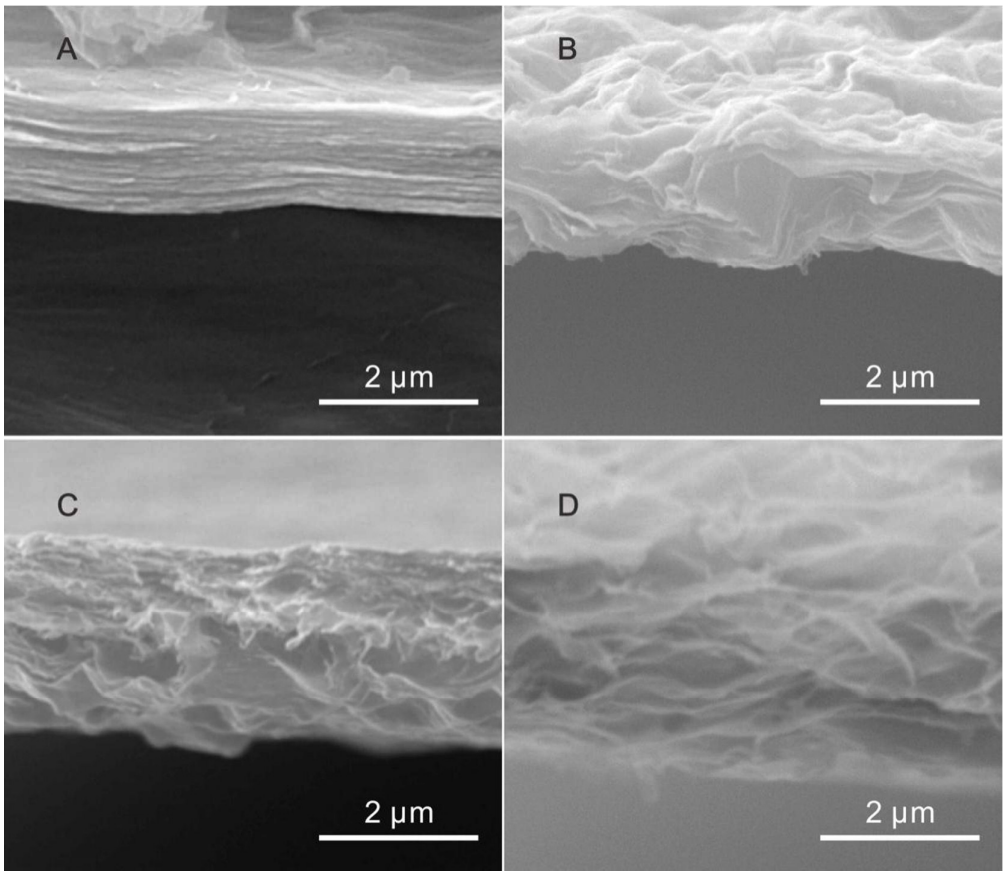

Figure 5. Typical SEM images of the cross-section of (A) RGO, (B) Ag2G1, (C) Ag5G1 and (D) Ag10G1.

To further characterize the Ag nanoparticle size on RGO sheet, TEM measurement was applied. The contents of Ag nanoparticles increased gradually as the silver concentration increased. Although Ag nanoparticles aggregated in some extents (Fig. 4), the Ag nanoparticles size distribution is similar for Ag5G1 and Ag10G1 composites, which is about 120 ± 60 nm (Fig. 6).

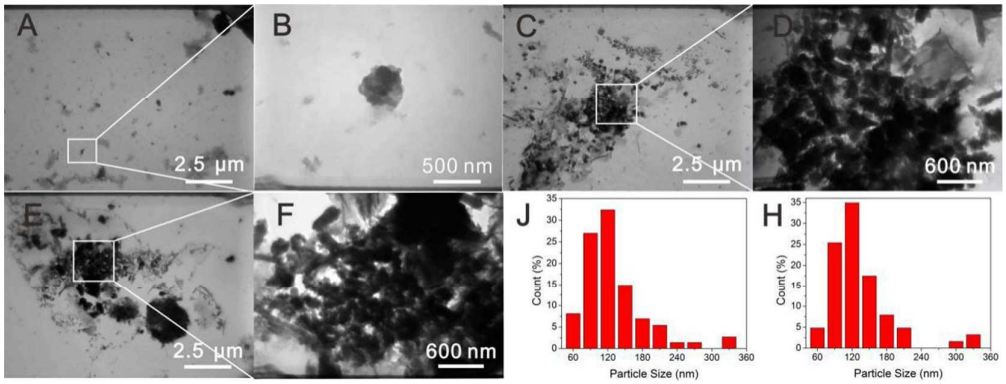

Figure 6. Typical TEM images of Ag2G1 (A, B), Ag5G1 (C, D), Ag10G1 (E, F) at low-magnification and high-magnification; Particle size distribution for Ag nanoparticles in Ag5G1 (J) and Ag10G1 (H) composites.

The electrical conductivity of the RGO/silver composite film was also measured by four-point probe. After L-AA/water vapor treatment, RGO films show an electrical conductivity of 3500 S m^{-1}, which is lower than that of hydrazine reduced graphene oxide but remarkably higher than that of solvothermally reduced graphene oxide which was carried out in NMP under oxygen-free condition [50, 51]. For RGO/silver composites, the electrical conductivity is 5250 S m^{-1}, 10500 S m^{-1}, and 35000 S m^{-1}, for Ag2G1, Ag5G1, and Ag10G1, respectively. The increased electrical conductivity also indicates the successful reduction of silver ion into silver nanoparticles. The Ag nanoparticles between the RGO films can hinder the restacking of RGO sheets, which is crucial for the good electrical conductivity of RGO film. Importantly, the Ag nanoparticles significantly decreased the resistance of the RGO film, likely due to the Ag nanoparticles decorating defect sites of RGO sheet and providing conductive paths [52].

3.3 SERS property of the RGO/Ag composites

As silver nanoparticles can enhance Raman signal, the SERS effect of RGO/Ag composites were investigated (Fig. 7). Compared to bare RGO films, the intensity of D and G band were enhanced about one times for Ag2G1 and four times for Ag10G1 (Fig. 7A). This enhancement is comparable to the result of Ag nanoparticles/RGO

systems reduced by hexamethylenetetramine at 180 ºC [53] and two times smaller than that of Ag/RGO systems by using hydrazine monohydrate as reducing agent [54].

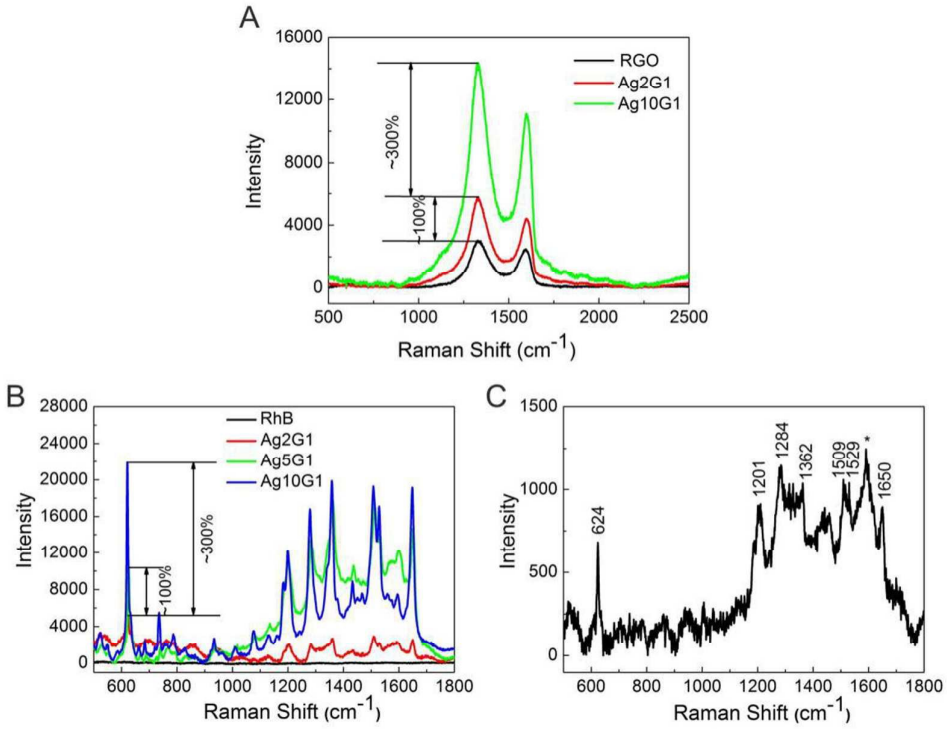

Figure 7. (A) Raman spectra of RGO , Ag2G1 and Ag10G1 films; (B) SERS spectra of 10^{-3} M RhB solution, RhB adsorbed on the Ag2G1, Ag5G1 and Ag10G1 substrate; and (C) 10^{-6} M RhB adsorbed on the Ag10G1 substrate, * marks the G band of graphene.

Furthermore we use RhB as probe molecule to demonstrate the SERS of the composites. The Raman spectra of RhB with the same concentration on Ag2G1, Ag5G1 and Ag10G1, were detected and shown in Figure 7B. In detail, the 1362, 1509 and 1650 cm^{-1} peaks are attributed to aromatic C-C stretching; 1284 cm^{-1} is assigned to aromatic C-C bridge-band stretching; 1201 cm^{-1} corresponding to aromatic C-H bending and 624 cm^{-1} corresponding to aromatic bending [55]. It is seen that the signal of RhB is hardly detected due to the feeble SERS activity of low concentration of RhB. Compared to the case of Ag2G1, the intensity at 624 cm^{-1} were enhanced about

1 times for Ag5G1, and 3 times for Ag10G1. There are two accepted independent proposals explaining the possible origin of enhancement: (I) electromagnetic enhancement and (II) chemical enhancement [56]. In our case, silver nanoparticles adsorbed on RGO sheets could use the attached functional groups as nucleation centers. Such interaction may form the charge-transfer complexes, which can absorb light at the excitation frequency, consequently producing chemical SERS. The detection limit was also measured for Ag10G1 films. When the concentration is decreased to 1 μM, all signals of RhB are observed, indicating high efficiency of SERS properties (Fig. 7C).

3.4 Antibacterial activity

Considering that the whole processes of reduction are green and no toxic agents are used, the antibacterial activities of RGO/Ag composites were determined by disc diffusion method. Figure 8 presents the antibacterial activities of various films against *E. coli* and *S. aureus* and *white-rot fungi*. The diameter of the zone of inhibition around the disk could be used to evaluate the antibacterial activity. It can be seen that RGO has no antibacterial activity against all bacteria (Fig. 8A), which is consistent with the previous report that the antibacterial activity is only due to the Ag nanoparticles [57,58]. Ag5G1 possesses much better antibacterial activity than Ag2G1 film, which is due to the incorporation of Ag nanoparticles. After more Ag nanoparticles are incorporated, Ag10G1 films exhibit much better antibacterial activity against *E. coli* and *S. aureus* than Ag2G1 and Ag5G1 films.

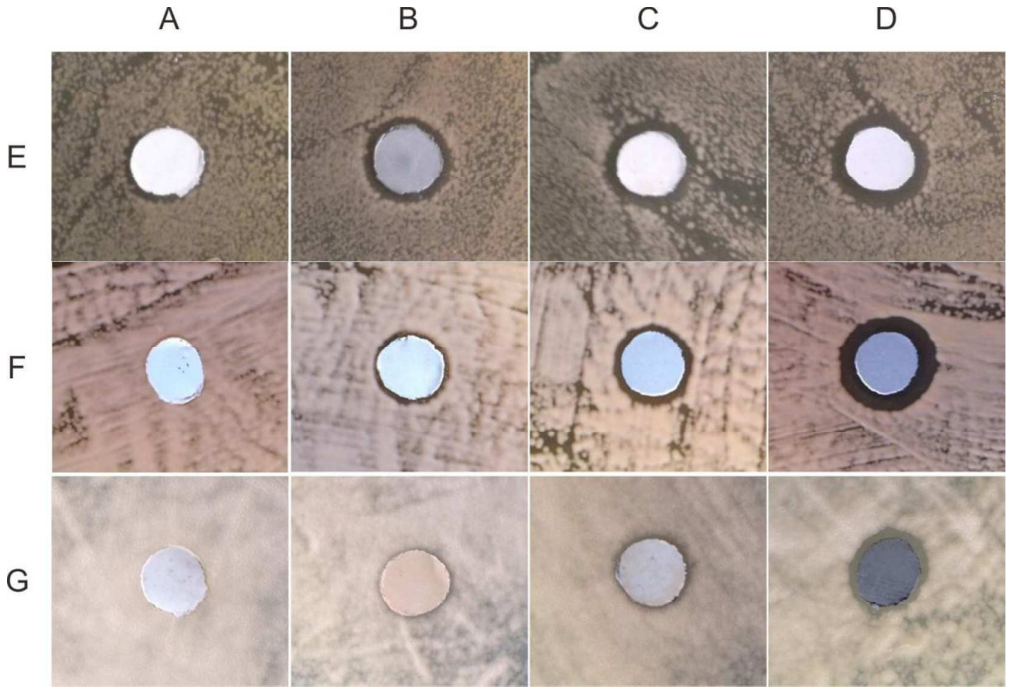

Figure 8. Inhibition zones of (A) RGO, (B) Ag2G1, (C) Ag5G1 and (D) Ag10G1 against (E) E. Coli, (F) S. aureus and (G) White-rot fungi.

There are three usually proposed possible mechanism of antibacterial action of silver nanoparticles: (I) gradual release of Ag^+, which then affects DNA replication and ATP production, (II) direct damage to cell membranes by Ag nanoparticles, (III) generation of reactive oxygen from Ag nanoparticle and Ag^+ [59]. In our case, Ag nanoparticles reduced from L-AA/water vapor could be changed into Ag^+ with the aid of air or water. After absorbing water during cultivation process, Ag nanoparticles or Ag^+ diffuse from the surfaces of the RGO/Ag composites to the bacteria on the agar plate. When Ag nanoparticles or Ag^+ contact with the bacteria, they either kill the bacteria or inhibit their growth.

Due to the similar size of Ag nanoparticles as revealed by TEM images, antibacterial activity of the composites mainly depends on the contents of Ag nanoparticles. Additionally, it was observed that Gram-negative *E. coli* was comparatively more sensitive to the Ag nanoparticles and produced maximum growth inhibition zone. While for *white-rot fungi*, only Ag10G1 revealed antibacterial

behavior.

4. Conclusion

A green and facile approach to prepare RGO films based on L-ascorbic acid/water vapor treatment is reported. The merit of this method is that pure flexible RGO films without any impurities are obtained and the reducing agents are environmentally friendly. Furthermore, silver ions attached on the GO films are also reduced into silver nanoparticles by this green method. The RGO/silver composites exhibit efficient SERS enhancement. The Raman signals can be tuned by changing the density of silver nanoparticles. Moreover, the composites also reveal antibacterial ability. High Ag loading on RGO/Ag composites shows better antibacterial for *E. coli*, *S. aureus*, and *white-rot fungi* bacteria. The as-synthesized RGO/Ag composites have great potential used as detection of small molecules and selective antibacterial nanomaterials.

Acknowledgments

The financial supported by Program for Scientific Research Innovation Team in Colleges and Universities of Shandong Province, the National Natural Science Foundation of China (21204044, 21176147 and 21276149), Shandong Outstanding Young Scientist Award Fund (BS2012CL028) and Ji'nan Overseas Students Pioneer Plan (20120202) are gratefully acknowledged.

Table of Contents

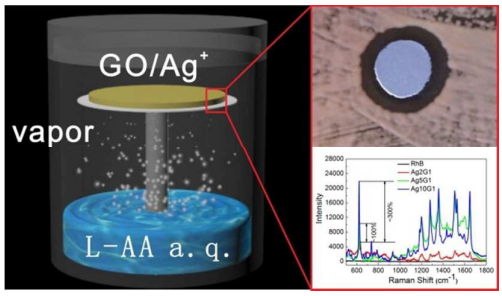

Free-standing RGO/Ag composite films with different Ag contents not only possess high Raman enhancement but also have antibacterial activity.

References

1. A. K. Geim, *Science*, 2009, **324**, 1530.
2. A. K. Geim and K. S. Novoselov, *Nat. Mater.*, 2007, **6**, 183.
3. V. Singh, D. Joung, L. Zhai, S. Das, S. I. Khondaker and S. Seal, *Prog. Mater. Sci.*, 2011, **56**, 1178.
4. K. S. Novoselov, V. I. Fal'ko, L. Colombo, P. R. Gellert, M. G. Schwab and K. Kim, *Nature*, 2012, **490**, 192.
5. X. Sun, H. Sun, H. Li and H. Peng, *Adv. Mater.*, 2013, **25**, 5153.
6. L. M. Dai, *Acc. Chem. Res.*, 2013, **46**, 31.
7. K. S. Novoselov, A. K. Geim, S. V. Morozov, D. Jiang, Y. Zhang, S. V. Dubonos, I. V. Grigorieva and A. A. Firsov, *Science*, 2004, **306**, 666.
8. K. S. Kim, Y. Zhao, H. Jang, S. Y. Lee, J. M. Kim, K. S. Kim, J. H. Ahn, P. Kim, J. Y. Choi and B. H. Hong, *Nature*, 2009, **457**, 706.
9. C. Berger, Z. M. Song, X. B. Li, X. S. Wu, N. Brown, C. Naud, D. Mayou, T. B. Li, J. Hass, A. N. Marchenkov, E. H. Conrad, P. N. First and W. A. de Heer, *Science*, 2006, **312**, 1191.
10. Y. Zhang, L. Y. Zhang and C. W. Zhou, *Acc. Chem. Res.*, 2013, **46**, 2329.
11. Y. Hernandez, V. Nicolosi, M. Lotya, F. M. Blighe, Z. Y. Sun, S. De, I. T. McGovern, B. Holland, M. Byrne, Y. K. Gun'ko, J. J. Boland, P. Niraj, G. Duesberg, S. Krishnamurthy, R. Goodhue, J. Hutchison, V. Scardaci, A. C. Ferrari and J. N. Coleman, *Nat. Nanotechnol.*, 2008, **3**, 563.
12. S. Park and R. S. Ruoff, *Nat. Nanotechnol.*, 2009, **4**, 217.
13. C. K. Chua and M. Pumera, *Chem. Soc. Rev.*, 2014, **43**, 291.
14. I. K. Moon, J. Lee, R. S. Ruoff and H. Lee, *Nat. Commun.*, 2010, **1**,1.
15. M. C. Kim, G. S. Hwang and R. S. Ruoff, *J. Chem. Phys.*, 2009, **131**,064704.
16. X. C. Dong, C. Y. Su, W. J. Zhang, J. W. Zhao, Q. D. Ling, W. Huang, P. Chen and L. J. Li, *Phys. Chem. Chem. Phys.*, 2010, **12**, 2164.
17. S. Mao, K. H. Yu, S. M. Cui, Z. Bo, G. H. Lu and J. H. Chen, *Nanoscale*, 2011, **3**, 2849.

18. P. Cui, J. Lee, E. Hwang and H. Lee, *Chem. Commun.*, 2011, **47**, 12370.
19. S. Stankovich, D. A. Dikin, R. D. Piner, K. A. Kohlhaas, A. Kleinhammes, Y. Jia, Y. Wu, S. T. Nguyen and R. S. Ruoff, *Carbon*, 2007, **45**, 1558.
20. H. D. Peng, L. Meng, L. Niu and Q. Lu, *J. Phys. Chem. C*, 2012, **116**, 16294.
21. C. Zhu, S. Guo, Y. Fang and S. Dong, *ACS Nano*, 2010, **4**, 2429.
22. Z. Bo, X. Shuai, S. Mao, H. Yang, J. Qian, J. Chen, J. Yan and K. Cen, *Sci. Rep.*, 2014, **4**,4684.
23. J. Liu, S. Fu, B. Yuan, Y. Li and Z. Deng, *J. Am. Chem. Soc.*, 2010, **132**, 7279.
24. H. A. Becerril, J. Mao, Z. Liu, R. M. Stoltenberg, Z. Bao and Y. Chen, *ACS Nano*, 2008, **2**, 463.
25. S. Pei, J. Zhao, J. Du, W. Ren and H. M. Cheng, *Carbon*, 2010, **48**, 4466.
26. B. Krautler, *Biochem. Soc. Trans.*, 2005, **33**, 806.
27. G. S. Métraux, Y. C. Cao, R. Jin and C. A. Mirkin, *Nano Lett.*, 2003, **3**, 519.
28. J. Zhang, H. Yang, G. Shen, P. Cheng, J. Zhang and S. Guo, *Chem. Commun.*, 2010, **46**, 1112.
29. P. Song, X. Zhang, M. Sun, X. Cui and Y. Lin, *RSC. Adv.*, 2012, **2**, 1168.
30. D. Wan, C. Yang, T. Lin, Y. Tang, M. Zhou, Y. Zhong, F. Huang and J. Lin, *ACS Nano*, 2012, **6**, 9068.
31. L. Q. Xu, W. J. Yang, K. G. Neoh, E. T. Kang and G. D. Fu, *Macromolecules*, 2010, **43**, 8336.
32. J. I. Paredes, S. Villar-Rodil, A. Martinez-Alonso and J. M. D. Tascón, *Langmuir,* 2008, **24**, 10560.
33. S. Park, D. A. Dikin, S. T. Nguyen and R. S. Ruoff, *J. Phys. Chem. C*, 2009, **113**, 15801.
34. Y. Gao, L. Q. Liu, S. Z. Zu, K. Peng, D. Zhou, B. H. Han and Z. Zhang, *ACS Nano*, 2011, **5**, 2134.
35. V. C. Tung, M. J. Allen, Y. Yang and R. B. Kaner, *Nat. Nanotechnol.*, 2009, **4**, 25.
36. Y. Zhou, Q. Bao, L. A. L. Tang, Y. Zhong and K. P. Loh, *Chem. Mater.*, 2009, **21**, 2950.
37. M. J. Fernández-Merino, L. Guardia, J. I. Paredes, S. Villar-Rodil, P.

Solis-Fernández, A. Martinez-Alonso and J. M. D. Tascón, *J. Phys. Chem. C*, 2010, **114**, 6426.

38. D. R. Dreyer, S. Park, C. W. Bielawski and R. S. Ruoff, *Chem. Soc. Rev*., 2010, **39**, 228.
39. B. Wen, X. X. Wang, W. Q. Cao, H. L. Shi, M. M. Lu, G. Wang, H. B. Jin, W. Z. Wang, J. Yuan and M. S. Cao, *Nanoscale*, 2014, **6**, 5754.
40. M. Ambrosi, E. Fratini, V. Alfredsson, B. W. Ninham, R. Giorgi, P. Lo Nostro and P. Baglioni, *J. Am. Chem. Soc.*, 2006, **128**, 7209.
41. J. Gao, F. Liu, Y. L. Liu, N. Ma, Z. Q. Wang and X. Zhang, *Chem. Mater.*, 2010, **22**, 2213.
42. G. Goncalves, P. A. A. P. Marques, C. M. Granadeiro, H. I. S. Nogueira, M. K. Singh and J. Grácio, *Chem. Mater.*, 2009, **21**, 4796.
43. W. Ren, Y. Fang and E. Wang, *ACS Nano*, 2011, **5**, 6425.
44. Z. Lin, Y. Yao, Z. Li, Y. Liu, Z. Li and C. P. Wong, *J. Phys. Chem. C*, 2010, **114**, 14819.
45. Q. Zhuo, J. Gao, M. Peng, L. Bai, J. Deng, Y. Xia, Y. Ma, J. Zhong and X. Sun, *Carbon*, 2013, **52**, 559.
46. A. V. Murugan, T. Muraliganth and A. Manthiram, Rapid, *Chem. Mater.*, 2009, **21**, 5004.
47. Z.L. Song, Z. Chen, X. Bian, L.Y. Zhou, D. Ding, H. Liang, Y.X. Zou, S.S. Wang, L. Chen, C. Yang, X.B. Zhang and W. Tan, *J. Am. Chem. Soc.*, 2014, **136**, 13558.
48. T. Wu, S. Liu, Y. Luo, W. Lu, L. Wang and X. Sun, *Nanoscale*, 2011, **3**, 2142.
49. S. Liu, J. Wang, J. Zeng, J. Ou, Z. Li, X. Liu and S. Yang, *J. Power Sources*, 2010, **195**, 4628.
50. D. Li, M. B. Müller, S. Gilje, R. B. Kaner and G. G. Wallace, *Nat. Nanotechnol.*, 2008, **3**, 101.
51. S. Dubin, S. Gilje, K. Wang, V. C. Tung, K. Cha, A. S. Hall, J. Farrar, R. Varshneya, Y. Yang and R. B. Kaner, A One-Step, *ACS Nano*, 2010, **4**, 3845.
52. R. S. Sundaram, C. Gómez-Navarro, K. Balasubramanian, M. Burghard and K.

Kern, *Adv. Mater.*, 2008, **20**, 3050.

53. B.K. Barman, K.K. Nanda, *RSC Advances*, 2014, **4**, 44146.

54. Z. Xu, H. Gao and H. Guoxin, *Carbon*, 2011, **49**, 4731.

55. Y. Zhao, W. Zeng, Z. Tao, P. Xiong, Y. Qu and Y. Zhu, *Chem. Commun.*, 2015, **51**, 866.

56. Q. Huang, J. Wang, W. Wei, Q. Yan, C. Wu and X. Zhu, *Journal of Hazardous Materials*, 2015, **283**, 123.

57. Z. Fan, B. Liu, J. Wang, S. Zhang, Q. Lin, P. Gong, L. Ma and S. Yang, *Adv. Funct. Mater.*, 2014, **24**, 3933.

58. L. Dellieu, E. Lawarée, N. Reckinger, C. Didembourg, J.J. Letesson, O. Deparis, J.Y. Matroule and J.F. Colomer , *Carbon*, 2015, **84**, 310.

59. A. Taglietti, Y.A.D. Fernandez, E. Amato, L. Cucca, G. Dacarro, P. Grisoli, V. Necchi, P. Pallavicini, L. Pasotti and M. Patrini, *Langmuir*, 2012, **28**, 8140.

Supporting Information

Green synthesis of graphene-silver composites reduced by L-ascorbic acid/water vapor for SERS enhancement and antibacterial application

Jian Liu[a], Libin Liu[a]*, Xiwen Wu[a], Xiaokai Zhang[b], Tianduo Li[a]*

[a] Shandong Provincial Key Laboratory of Fine Chemicals, Key Laboratory of Fine Chemicals in Universities of Shandong, Qilu University of Technology，Jinan 250353, China

E-mail: lbliu@qlu.edu.cn (Prof. L. B. Liu); litianduo@163.com (Prof. T. D. Li)

[b] Institute of Semiconductors, Shandong Normal University, No. 88 East Culture Road, Jinan, China

Materials Characterization

UV-Vis absorption spectra were recorded on a UV-2600 UV-vis spectrometer (Shimadzu, Japan). Fourier-transform infrared spectroscopy (FT-IR) spectra were obtained on a FT-IR spectrometer IR Prestige-21 (Shimadzu, Japan). X-ray diffraction (XRD) analyses of the GO, RGO and RGO/Ag samples were carried out on a D-8 ADVANCE X-ray diffractometer (Bruker AXS, Germany) with graphite monochromatized Cu Kα irradiation (λ = 1.54 Å) with a voltage of 40 kV and current of 40 mA. Thermogravimetric analysis (TGA) was conducted in a continuous nitrogen flow with a flow rate of 150 mL min^{-1} and a heating rate of 10 °Cmin^{-1} from room temperature to 850 °C using a SDT Q600 (TA, America). X-ray photoelectron spectroscopy (XPS) measurements were taken in a ESCALAB 250 (Thermo Fisher Scientific, America) using a monochromatic Al-Kα X-ray source at 100 W. The

surface and cross-section images of the RGO/Ag films were characterized by scanning electron microscope (SEM) QUANTA 200 (FEI, America). The equilibrium contact angles (CA) were measured by a DSA 100 (KRÜSS, Germany) contact angle meter at ambient temperature. The morphology and microstructures were observed by transmission electron microscope (TEM) H-800 (HITACHI, Japan) at an accelerating voltage of 100 kV. Atomic force microscopy (AFM) images were taken on a Mutimode 8 Nanoscope V system (Bruker, USA) in peak force tapping mode. Electrical measurements were performed using a four-point probe measurement station (Jandel RM3-AR Test Meter with Multiheight Probe attachment), and the average of three data points per sample was recorded.

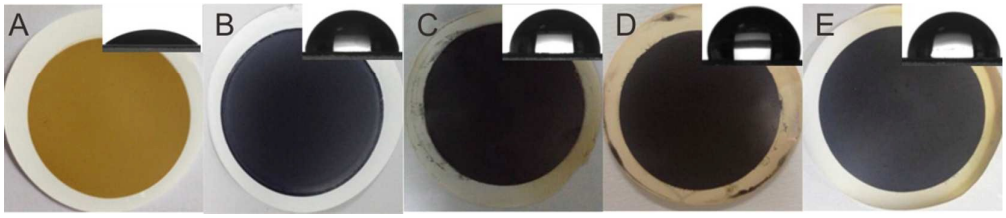

Figure S1. Pictures of (A) GO, (B) RGO, (C) Ag2G1, (D) Ag5G1 and (E) Ag10G1 films, and the equilibrium water contact angles: 37.2±0.5°, 88.8±0.5°, 98.2±0.5°, 106.5±0.5° and 97.3±0.5°, respectively.

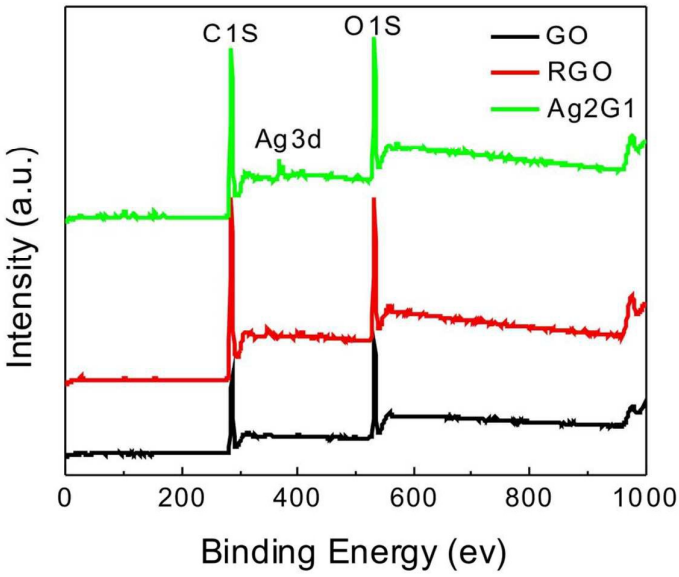

Figure S2. XPS survey spectra of the as-prepared GO and RGO and Ag2G1 composites.

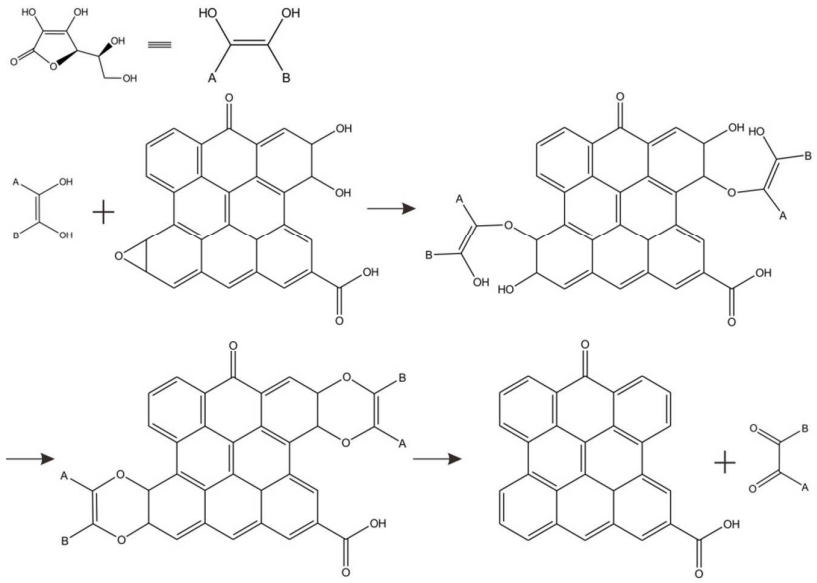

Figure S3. Reaction pathway for the chemical reduction of GO with L-AA.

Table of Contents

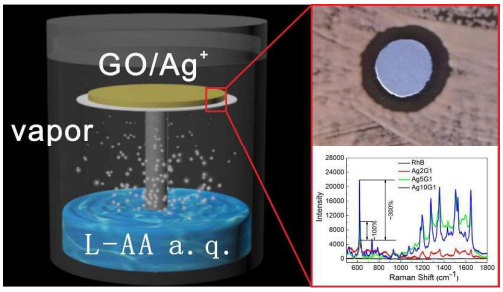

Free-standing RGO/Ag composite films with different Ag contents not only possess high Raman enhancement but also have antibacterial activity.